Comparisons between data recorded by several 3-component coil geophones and a MEMS sensor at the Violet Grove monitor seismic survey

Don C. Lawton, Malcolm B. Bertram, Gary F. Margrave and Eric V. Gallant.

ABSTRACT

During the Violet Grove CO_2 injection monitor seismic survey, several different 3-C coil geophones and a micro-electro mechanical system (MEMS) sensor were co-located at 8 adjacent stations along one of the receiver lines. The 3-C geophones were manufactured by Oyogeospace and Input/Output Inc., and the MEMS sensor was made by Sercel. The geophones were all fitted with elements with a natural frequency of 10Hz and 0.7 damping. The receiver line crossed a well lease that was covered with a mixture of gravel and dirt that was frozen at the time of the survey. The geophones and sensor were separated from one another by approximately 1 m within each group and the receiver group interval was 20 m across the well lease. A total of 225 shots were recorded for the experiment with a good distribution of source-receiver azimuths and a maximum offset of nearly 2 km.

Common receiver gathers for the vertical and radial components of the datasets were examined for this study. Geophone gathers were compared against each other and with MEMS sensor gathers both in raw form (MEMS devices provide accelerometer output) and after the latter were integrated so that all datasets represented measurements of particle velocity. Visual comparison of receiver gathers showed a very high degree of similarity. The correlation coefficient between gathers of geophone data exceeded 0.98 for most records and was only slightly less between geophones and MEMS sensors, with differences attributable to the phase distortion of geophone data across the resonant frequency. Amplitude spectra for the geophones and integrated MEMS sensor were also very similar. Data quality was consistent regardless of the style of ground coupling of the geophones or the sensor. Two different recording systems were used for the experiment (Sercel for the MEMS sensor and an ARAM Aries system for the geophone data) and some of the phase characteristics of the raw data are interpreted to be related to the instrument antialias filters implemented by the two systems, as well as phase distortions within the signal band of the recorded geophone data.

INTRODUCTION

Since the development of micro-electro mechanical system sensors (MEMS), there has been interest in comparisons between the performances of these devices from different manufacturers as well as between MEMS devices and conventional coil geophones (e.g. Tessman et al., 2001; Mougenot and Thorburn, 2004; Gibson et al., 2005a, 2005b; Ronen et al., 2005a, 2005b; Calvert et al., 2005). Most of these studies have compared data after processing through to stack. Gibson et al. (2005a) found insignificant difference in limited data comparisons between two different MEMS systems (Sercel DSU3 and IO Vectorseis). Ronen et al. (2005a) compared receiver gathers before stack and concluded that weather and shot repeatability appears to be a more significant contributor to differences that the sensor type. They also found the differences between processed

datasets to be small. One of the key advantages of the MEMS devices over conventional 3C coil geophones is efficiency in the field and certainty in the relative orientation of the horizontal elements due to fewer cabling requirements.

The monitor survey for a time-lapse, multicomponent seismic program at the Penn West CO_2 injection pilot at Violet Grove, Alberta was recorded by Veritas Geoservices in December 2005 using Sercel 408XL recording instruments with Sercel model DSU3 MEMS sensors. Since the University of Calgary had recently acquired a new ARAM Aries seismic recording system, and had access to several different types of 3-C coil geophones, it was decided to set up an experiment at several receiver stations at which these different types of coil geophones could record data simultaneously with the Sercel monitor survey. The objectives of the experiment were to compare the field performance of three different types of coil geophones with different planting styles, and to compare coil geophones with the Sercel DSU3 devices. Few previous studies have made comparisons between raw data collected by horizontal elements of these geophones and sensors. Although it is recognized that two different recording systems were used, the experiment provides value to resource companies who may wish to merge legacy datasets recorded using different devices.

FIELD EXPERIMENT

The Penn West CO_2 enhanced oil recovery pilot site is located in the Pembina oil field, about 80 km southwest of Edmonton. CREWES has developed a seismic monitoring strategy involving a sparse, multicomponent surface seismic program integrated with active and passive monitoring using geophones permanently cemented into an observation well (Figure 1). The surface seismic program provides 3D subsurface coverage of the pilot site whilst data from the downhole geophones provide high-resolution images around the observation well. The downhole geophone installation is being used for passive monitoring of CO_2 injection between active-source seismic surveys. The baseline survey was completed in March 2005 and results were presented by Lawton, 2005; Chen and Lawton, 2005; Coueslan et al., 2005). The first monitor survey was recorded in December 2005 and the time-lapse VSP results are discussed by Coueslan et al. (2006).

Because of the amount of geophone cabling required, the field experiment was located on the lease of the observation well along Line 5. The area is surfaced with a mix of gravel and earth and was frozen at the time of the survey. Eight receiver stations (5183 through 5190) at an interval of 20 m were each occupied with 3 different types of geophones, as listed in Table 1. The geophones at each receiver station were planted between 1.0 and 1.5 m apart in an east-west direction (perpendicular to the Line 5). A fourth type of geophone (Table 1) was included at two of the stations (5183 and 5184) as well as at the half station.

The layout geometry of the experiment is shown in Figure 2. The DSU3 sensors were connected through a single cable as part of the overall monitor survey. The coil geophones were all connected using three lines, one line for each component. All of the geophones were equipped with 10 Hz geophones and 0.7 damping.

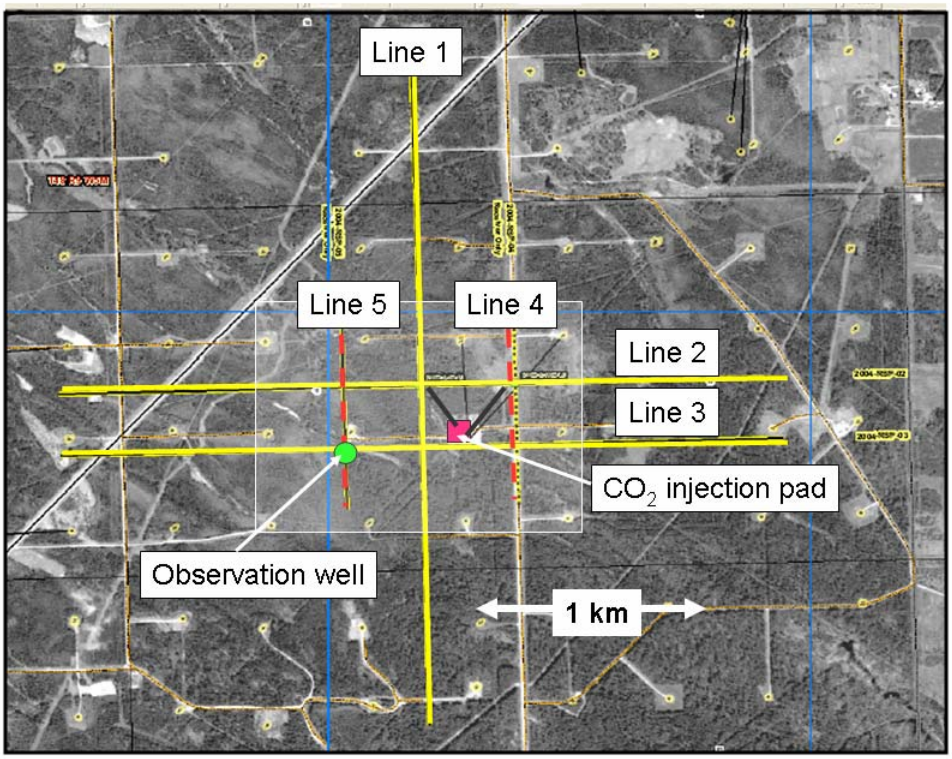

FIG. 1. Map showing Penn West CO_2 injection site. Multicomponent seismic lines (Lines 1, 2, 3) are shown in yellow, and receivers-only lines (Lines 4, 5) are shown in red. The geophones used in this experiment were located on Line 5 near the Observation well.

Table 1. Details of geophones used in the experiment.

Manufacturer	**Model**	**Element**	**Stations**
Input/Output	IO-Spike	SM24 (coil)	5183-5190
OyoGeospace	GS-3C	GS-20DM (coil)	5183-5190
Sercel	DSU3	MEMS	5183-5190
OyoGeospace	OG-Nail	GS-32CT (coil)	5183-5184

Figure 3 shows a photograph of the Sercel DSU3 sensor about to be deployed in the field, and Figure 4 is a photograph of the 3 coil geophones tested. Figure 5 shows the geophones deployed at station 5184. All geophones were oriented carefully. The DSU3 sensors were oriented with the H1 component pointing to magnetic South (bearing of 199.3^o), and all coil geophones were oriented with the H1 component oriented towards geographic 178^o which was the bearing of Line 5.

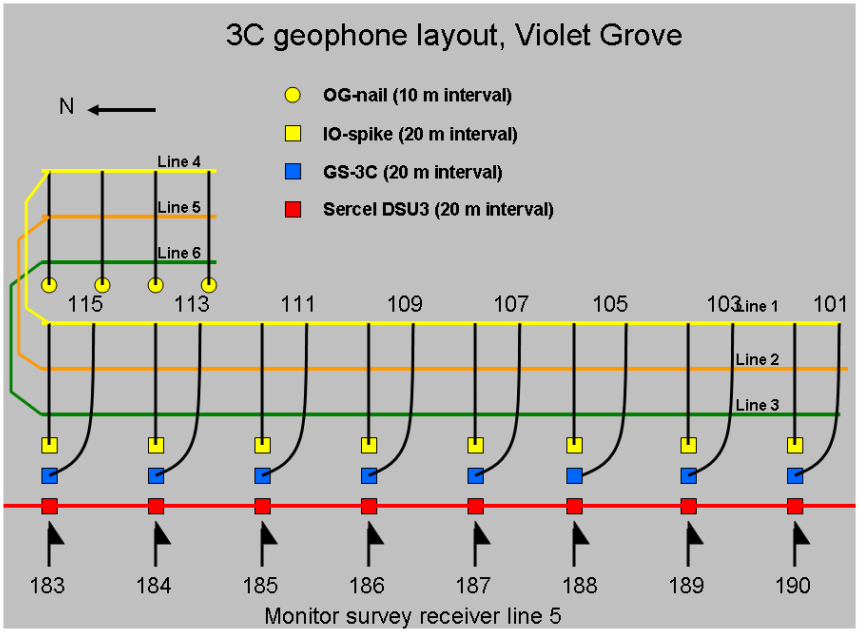

FIG. 2. Layout pattern of geophones and cabling system for the geophone/sensor comparison experiment.

FIG. 3. DSU3 sensor being prepared for layout.

FIG. 4. Coil geophones used in the experiment. GS-3C (left); IO-Spike (centre) and OG-Nail (right).

FIG. 5. Three of the geophones planted at station 5184. Order from bottom to top is Sercel DSU3, IO-Spike and GS-3C (IO-Nail is missing from this view).

The Sercel sensors were used as part of the monitor survey using a Sercel 408XL recording system. All of the coil geophones were cabled to the University's ARAM recording system which was operated in slave mode. A total of 225 shots from the monitor survey were recorded. A map showing all shots in the survey, as well as the locations of the 8 geophone stations occupied for this experiment is shown in Figure 6, with a more detailed view shown in Figure 7. As seen in Figures 6 and 7 a reasonably good distribution of source-receiver offsets and azimuths was recorded.

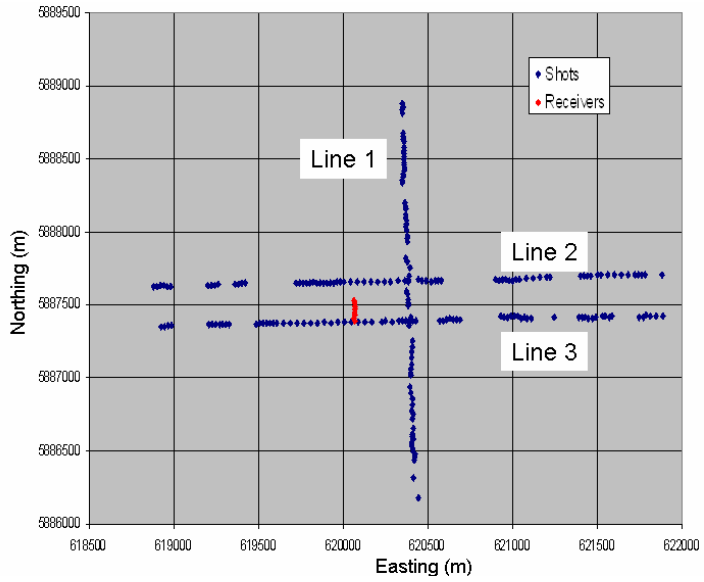

FIG. 6. All shots (blue) that were recorded by the geophones used in the experiment (red).

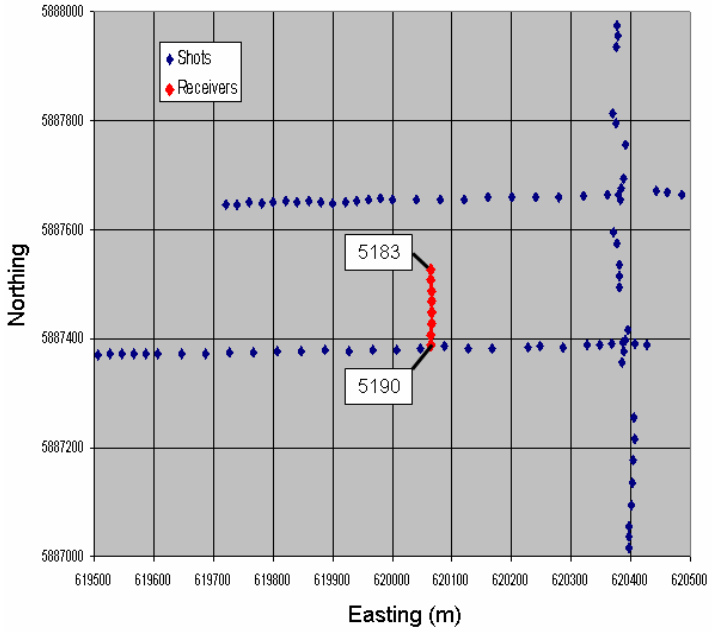

FIG. 7. Detailed view of the experimental layout, showing receiver stations (5183-5190) in red.

ANALYSIS

For the GS-3C, IO-Spike and Sercel DSU3 geophones, a total of 8 common receiver gathers were obtained for each component, with each gather containing 225 traces, over a range of offsets and azimuths. For the OG-Nail, 4 common receiver gathers were obtained, two on receiver stations and two at mid-station. The only processing applied initially to the data were a tilt correction for the Sercel data (undertaken by Veritas) and a geometric rotation of the recorded H1 and H2 components into radial and transverse components for all geophones, using the known source and receiver coordinates.

For the purposes of this paper, the analysis will focus on data recorded at station 5183 from all shots (75) along Line 1, for the vertical and radial components. The complete dataset will shortly be available to sponsors who may wish to undertake their own analyses. From work that we have done to date, observations from data collected at receiver station 5183 are very similar to those made at the other receiver stations.

Vertical Component data

Figures 8 through 11 show raw vertical-component receiver gathers recorded by the IO-Spike, GS-3C, OG-Nail and Sercel-DSU3 respectively. These displays have had AGC scaling with a 500 ms window applied and have been truncated to a record length of 2.5s. Data from all of the geophones are very similar and there are no significant differences apparent for different geophone coupling styles (e.g. spike vs nail).

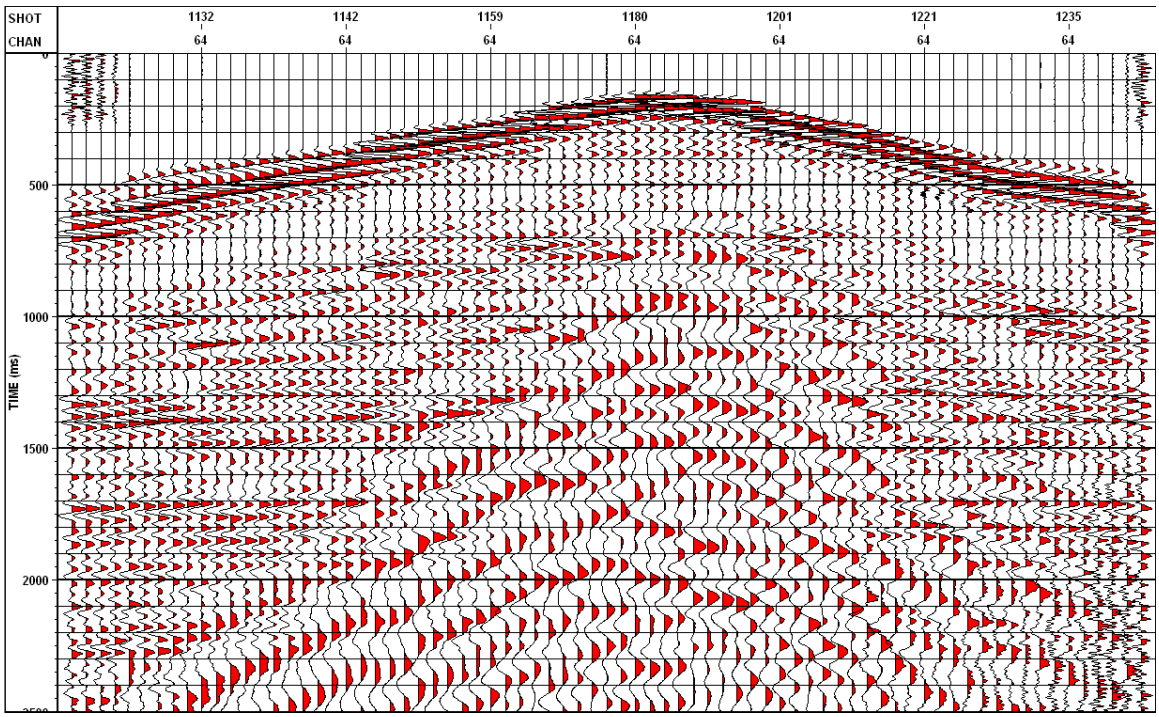

FIG. 8. Station 5183: IO-Spike vertical component with 500 ms window AGC applied.

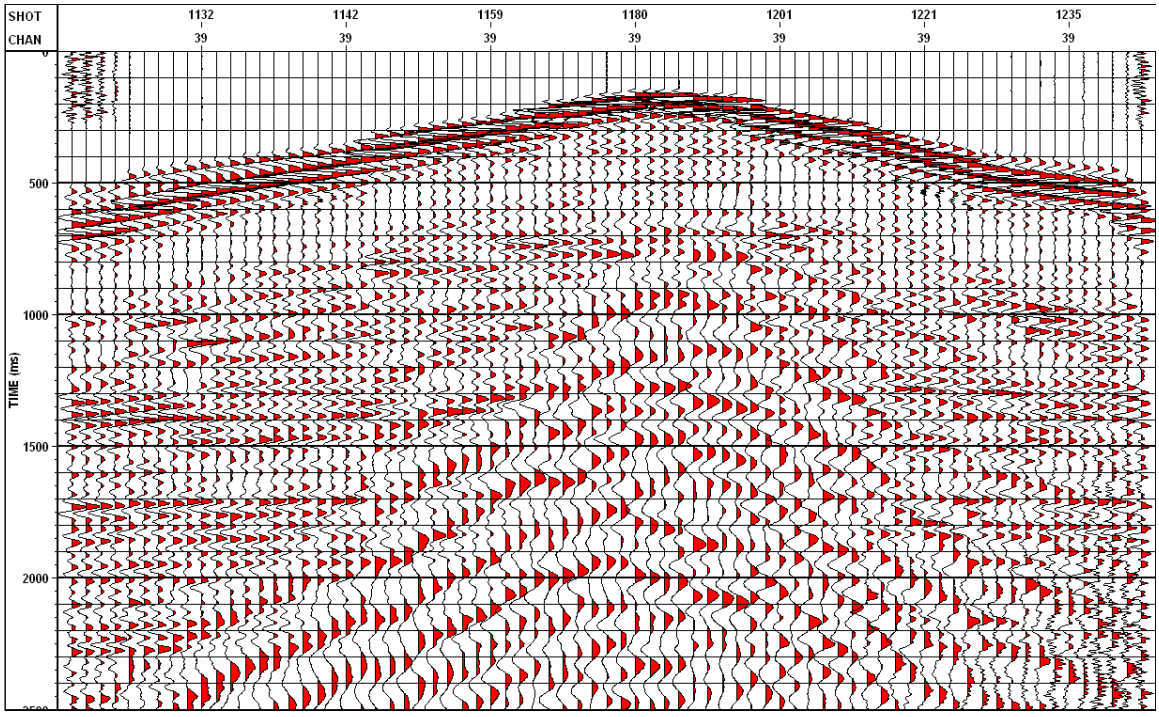

FIG. 9. Station 5183: GS-3C vertical component with 500 ms window AGC applied.

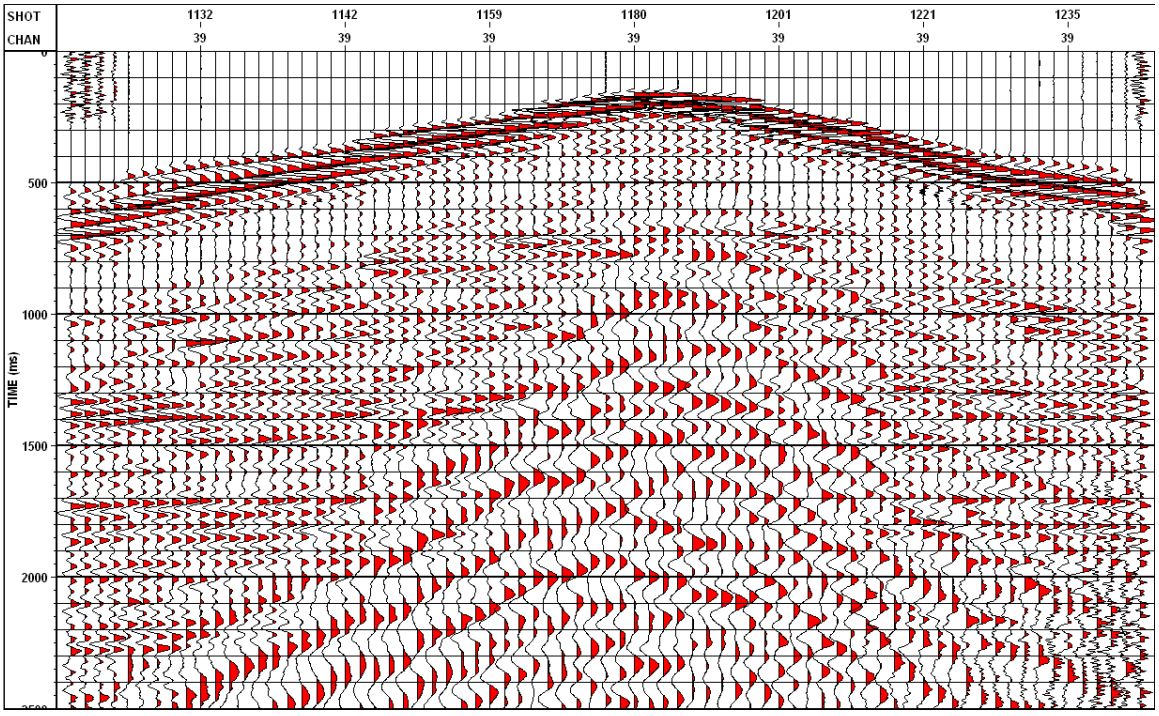

FIG. 10. Station 5183: OG-Nail vertical component with 500 ms window AGC applied.

.

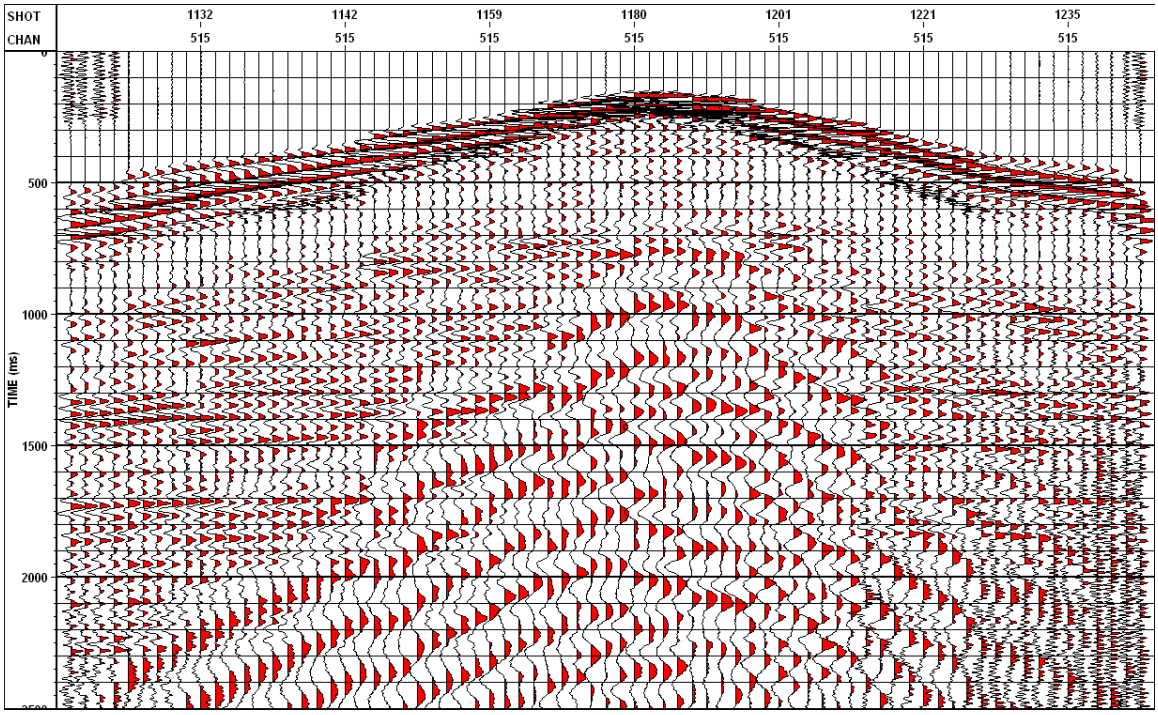

FIG. 11. Station 5183: Sercel-DSU3 vertical component with 500 ms window AGC applied.

The Sercel DSU3 is an accelerometer, and thus the raw data show higher amplitudes at higher frequencies (Figure 11) than the coil geophones, which measure velocity (Figures 8-10). Because the Sercel DSU3 measures acceleration and the coil geophones measure velocity, we had expected a 90^{o} phase difference between the raw data sets. However, inspection of traces from individual receiver gathers show that this is not obvious. Studies by Hon and Stewart (2006) show that this result may be caused by the geophone phase characteristics within the passband of the data recorded. It may also be caused in part by the application of a 0.8 Nyquist minimum-phase instrument filter used in the Sercel recording system for this survey compared with a zero-phase anti-alias filter used in the ARAM system. Figure 12 shows near-offset traces for a number of different shots, with traces from each geophone type juxtaposed within sub-gathers. In Figure 12a, 2 seconds of data are displayed, including first breaks, shallow reflections and surface waves. The first arrivals and shallow reflections have a very similar character across all traces; the low-frequency surface waves show a phase difference between the Sercel-DSU3 and the coil geophones. This is interpreted to be due the phase distortion by the coil geophones across resonance frequency (10 Hz). In Figure 12b we show detailed displays of the first breaks. The main first arrival wavelets are very similar and the DSU3 data show additional high-frequency events consistent with an accelerometer output.

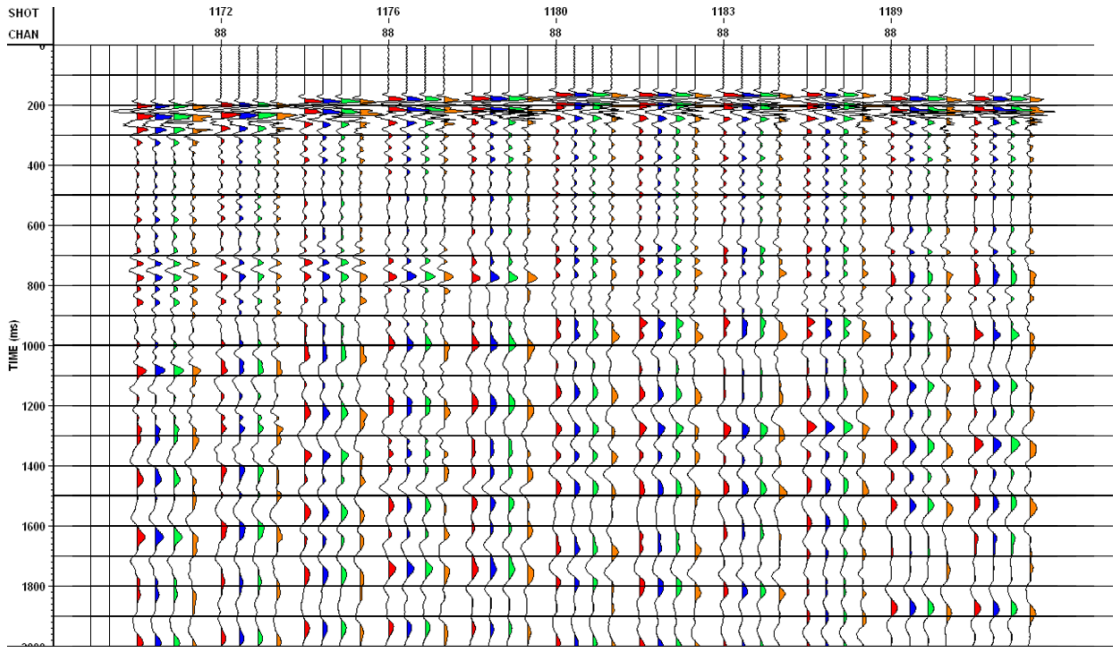

(a)

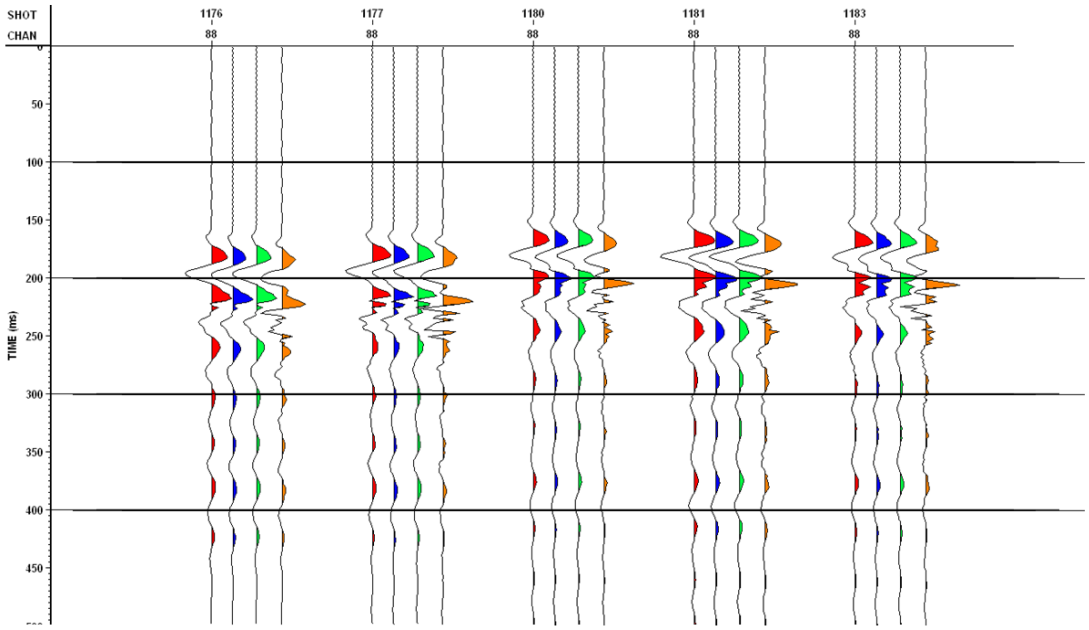

(b)

FIG. 12. Comparison of near offset traces, vertical component at station 5183. OG-Nail (red); IO-Spike (blue); GS-3C (green); Sercel-DSU3 (orange). (a) 2s of data, (b) detail of first breaks.

Figure 13 shows a similar set of sub-gathers to Figure 12, except for far offset traces. In this window, only first arrivals and reflections are recorded and all traces are very

similar, both for the full 2s of data (Figure 13a) and for the first-break details (Figure 13b). It is interesting to note that even the pre-first break noise is highly correlated.

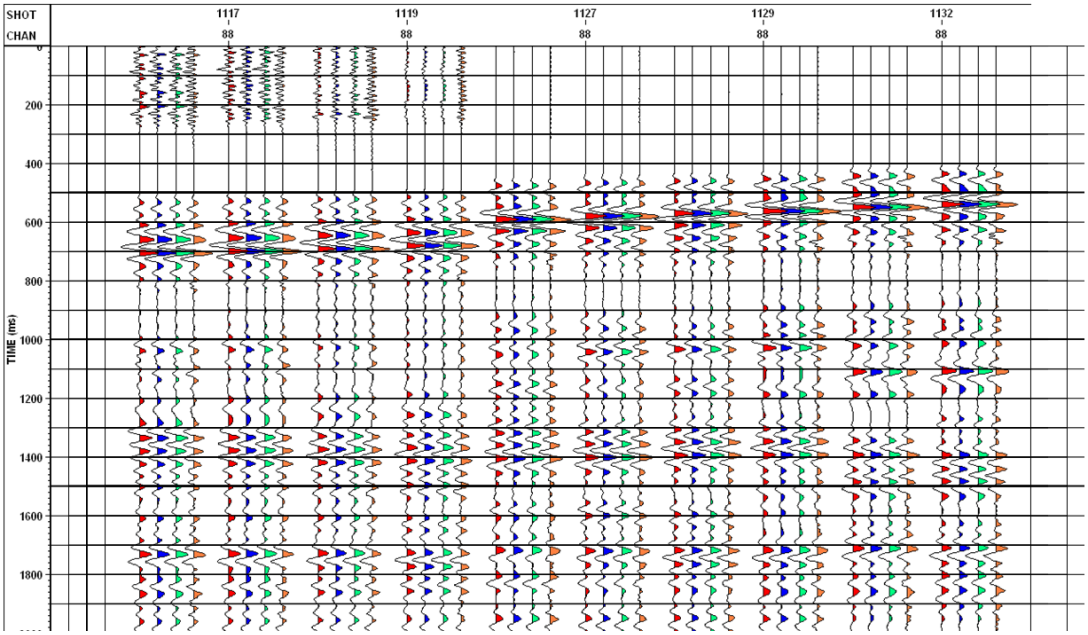

(a)

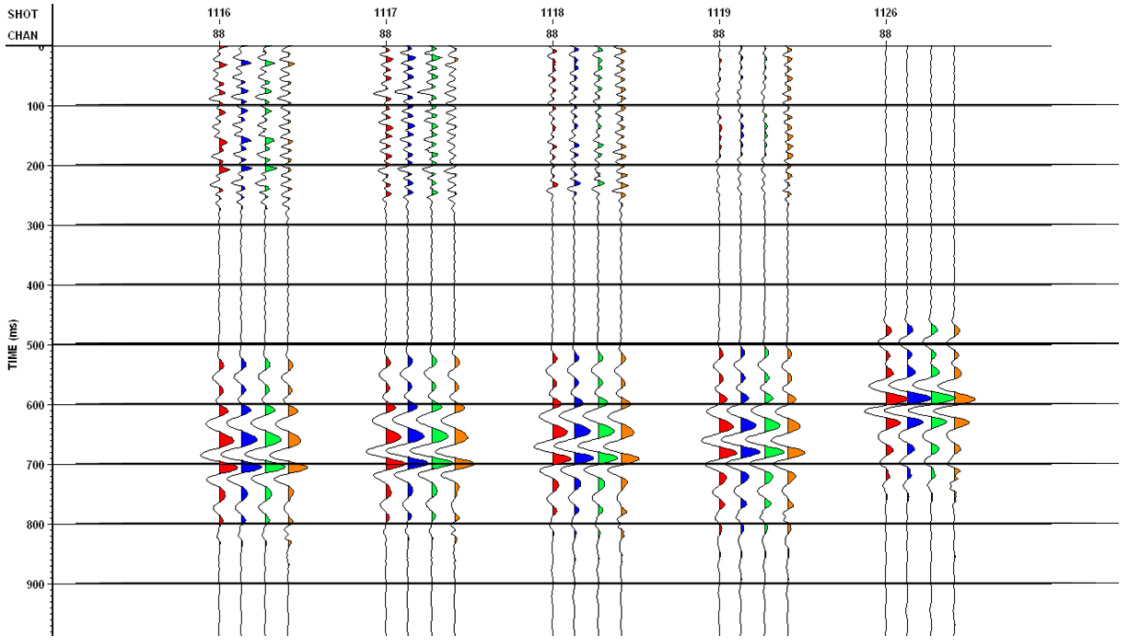

(b)

FIG. 13. Comparison of far-offset traces, vertical component at station 5183. OG-Nail (red); IO-Spike (blue); GS-3C (green); Sercel-DSU3 (orange). (a) 2s of data, (b) detail of first breaks.

As a further aid in interpretation of these results, a simple synthetic data experiment was conducted in MATLAB using tools in the standard CREWES library. Rather than attempt a simulation of the complex delta-sigma system, the synthetic data were simply generated at a sample rate of 0.0001 seconds and then resampled to 0.001 seconds using both zero-phase and minimum-phase antialias filters. A synthetic "velocity" trace, consisting of a single unit impulse in the middle of the trace was constructed and the corresponding "acceleration" trace was created by simple finite-difference differentiation. Then both traces were resampled, using both antialias filters, to create the four traces on the left of Figure 14. The 90 degree phase rotation is clearly evident if the velocity and acceleration traces are compared with the same type of antialias filter. However, the comparison most relevant to this study is the zero-phase antialias filter applied to the velocity trace (i.e. the first trace in the figure) and the minimum-phase filter applied to the acceleration trace (i.e. the fourth trace in the figure). In this case, the eye cannot distinguish a 90 degree phase rotation even though it is clearly there. The situation is even more complex when the traces are limited to a realistic signal band by convolution with a minimum phase wavelet having a dominant frequency of 20 Hz. As shown in the middle four traces in Figure 14, the 90 degree relation may still be discerned by a careful comparison of traces with the same type of antialias filter. On the other hand, comparison of the first and fourth traces of the middle panel shows the leading peaks are actually quite well aligned, which might lead to the interpretation that the data are "the same phase". Also of interest here is the jagged character of the first trough following the leading peak of the minimum-phase filtered acceleration trace. This may model some of the effects seen on the Sercel data. Finally, the four synthetic traces in the middle panel were passed through minimum-phase Wiener deconvolution and the results are on the right in Figure 14. Comparing either the first and third traces of the last panel or the second and fourth traces shows that deconvolution has corrected for the essential difference between the velocity and acceleration traces. This happens because the derivative operator is actually a minimum phase operator. Comparing the first and last traces after deconvolution is appropriate for the present experiment. The suggestion is that we might see a several millisecond time shift between the data; however, this is unlikely since a true zero-phase antialias filter cannot be implemented in causal instrumentation. Most likely the actual filter used was zero-phase plus delay or linear phase.

It may seem odd that a minimum-phase antialias filter, whose amplitude spectrum only begins to roll off at 80% of Nyquist could affect the phase of the data in the much lower signal band and so confuse the 90 degree phase rotation interpretation. The reason this can happen is that the phase of the antialias filter is actually strongly nonzero at all frequencies and happens to be about -90 degrees right in the signal band. Figure 15 shows the spectrum of the antialias filter used in this simulation. While this is certainly an oversimplification of what is really happening in a delta-sigma system, the similarity of the results to our observations suggests that it is an appropriate model.

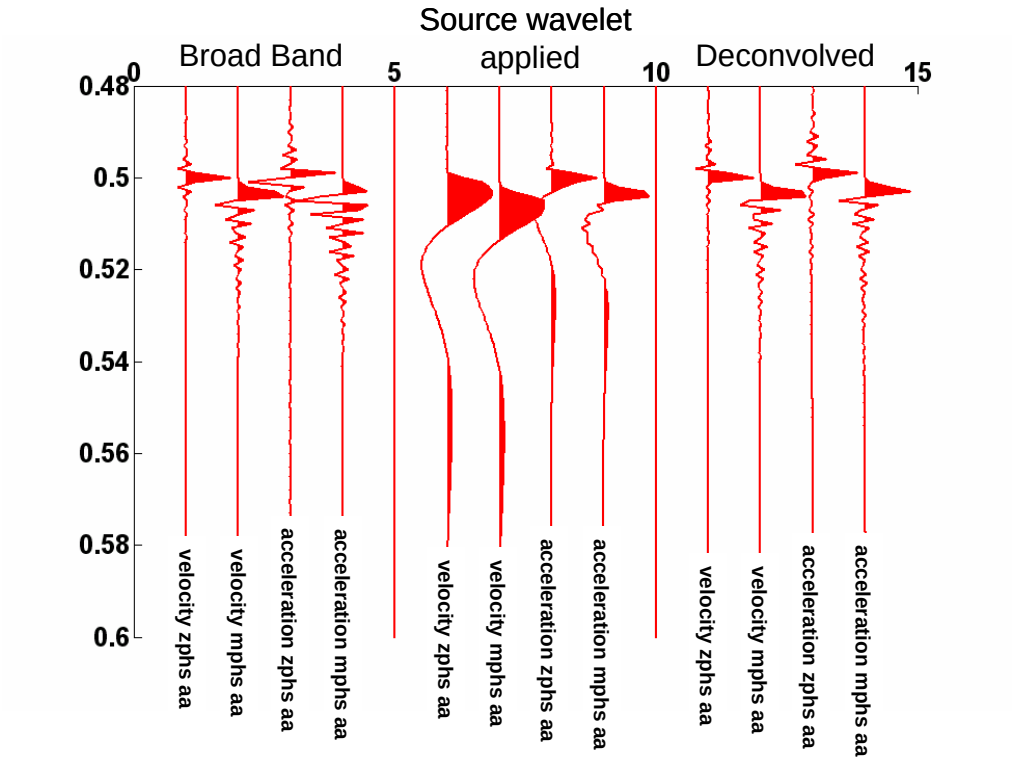

FIG. 14. From the left, traces 1 and 2 are the result of resampling a broad-band spike, representing an impulse in velocity, from 0.0001 seconds to 0.001 seconds using zero-phase and minimum-phase antialias filters. Traces 3-4 are the result of doing the same thing to the corresponding acceleration traces, created by differentiating the velocity trace. Traces 6-9 show the same four traces with a 20 Hz dominant frequency, minimum-phase wavelet applied. Traces 11-14 show the middle four traces after minimum-phase spiking deconvolution.

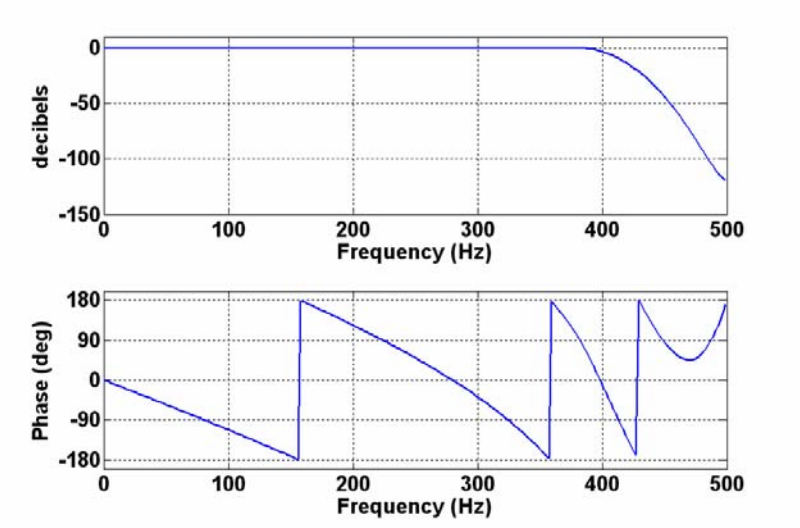

FIG. 15. The Amplitude spectrum (top) and phase spectrum (bottom) of the minimum-phase antialias filter used in the simulation shown in Figure 14.

In light of the discussion above and in order to provide a more direct comparison between the velocity (coil geophone) and acceleration (MEMS) data, the latter datasets were integrated followed by a 3 Hz low-cut filter and a phase-rotation of 90^o to compensate for the apparent phase rotation observed in the data. Figure 16 shows the vertical component of the DSU3 common receiver gather for shots from Line 1 after integration, and Figure 17 shows the same data after a 90^o phase rotation. These data are now very similar to the output from the coil geophones, a result that may in fact be somewhat fortuitous. A more rigorous approach that will be undertaken as this study continues will be to correct the geophone data for the appropriate phase response and also to properly compensate for the instrument anti-alias filter response. Broad-band events (e.g. first breaks and reflections) are very similar between the datasets, whereas the low-frequency surface waves have higher relative amplitude in the integrated Sercel data, as expected from the flat response of the Sercel instruments at low frequencies, essentially to DC.

Figure 18 shows a side-by-side view of part of the Sercel-DSU3 data after integration and a 90^o phase rotation and the equivalent part of the IO-Spike common receiver gather.

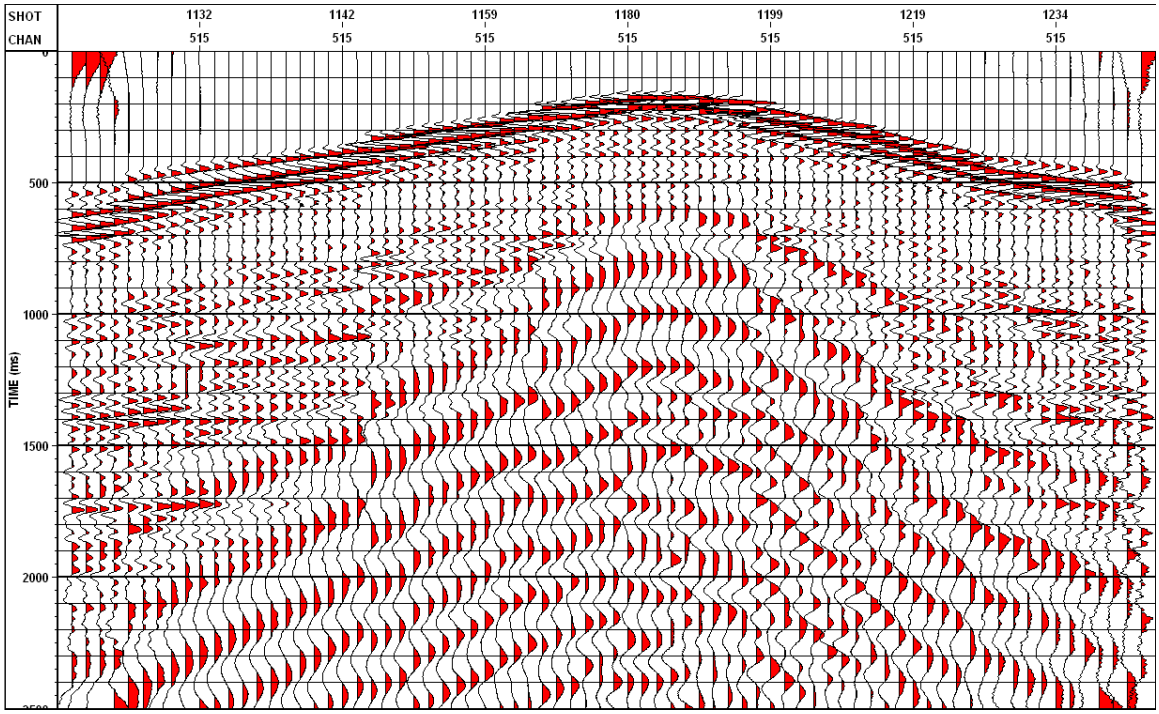

FIG. 16. Station 5183: Sercel-DSU3 vertical component integrated followed by a 3Hz low-cut filter. Display has a 500 ms window AGC applied.

To examine comparisons of reflection data, the common receiver gathers were filtered with a bandpass filter of 10-15-60-80 Hz. The gathers, in the same order as Figures 8 though 11 are displayed in Figures 19-22, respectively, except that for this comparison,

the Sercel data has been integrated and phase-rotated before filtering. The records are all very similar, with minor differences in reflection data recovered from beneath the surface waves for the Sercel-DSU3 data.

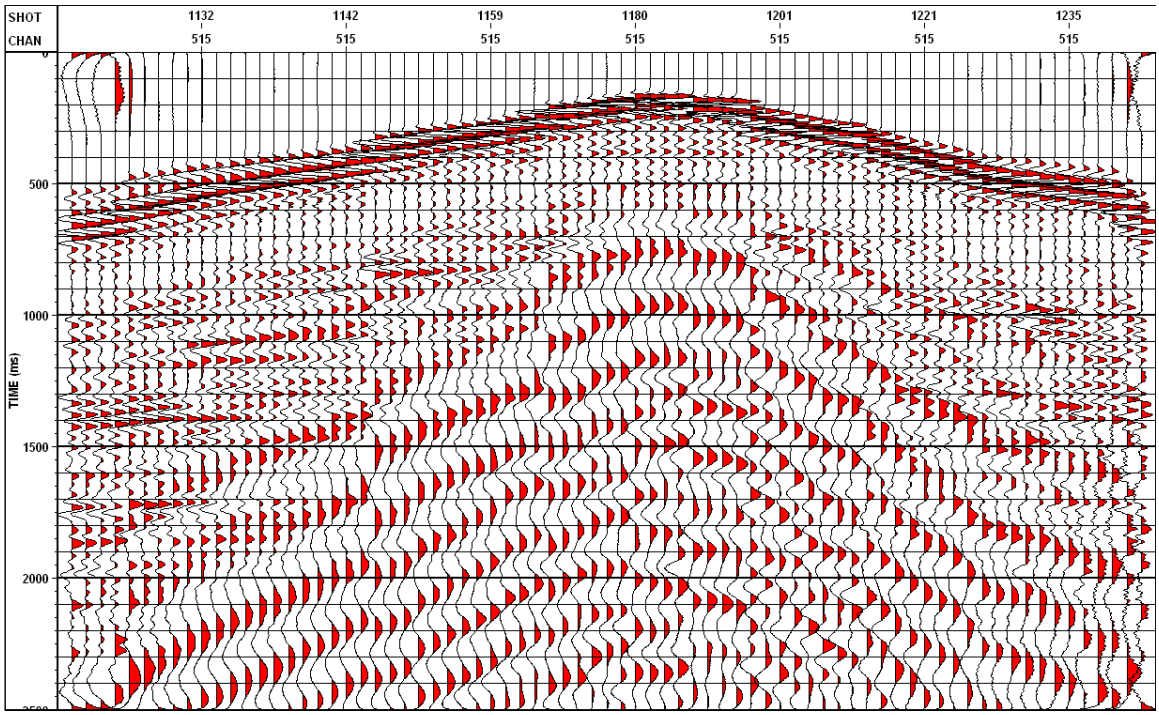

FIG. 17. Same data as in Fig. 14 except a 90^{o} phase rotation has been applied to the data.

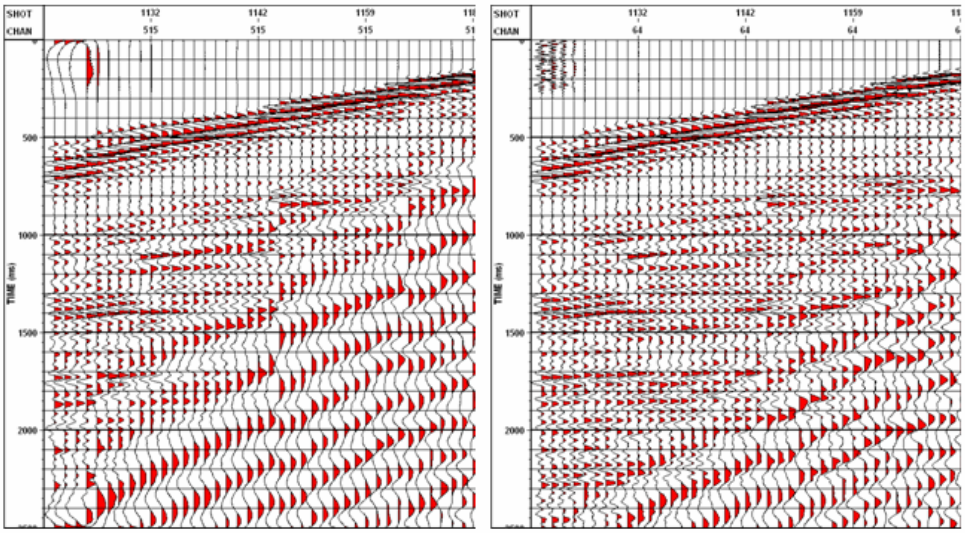

FIG. 18. DSU3 vertical-component gather after integration and 90^{o} phase shift (left) compared to equivalent traces from the IO-Spike gather (right). Note higher relative amplitudes of the surface waves in the DSU3 gather, but close similarity between reflections.

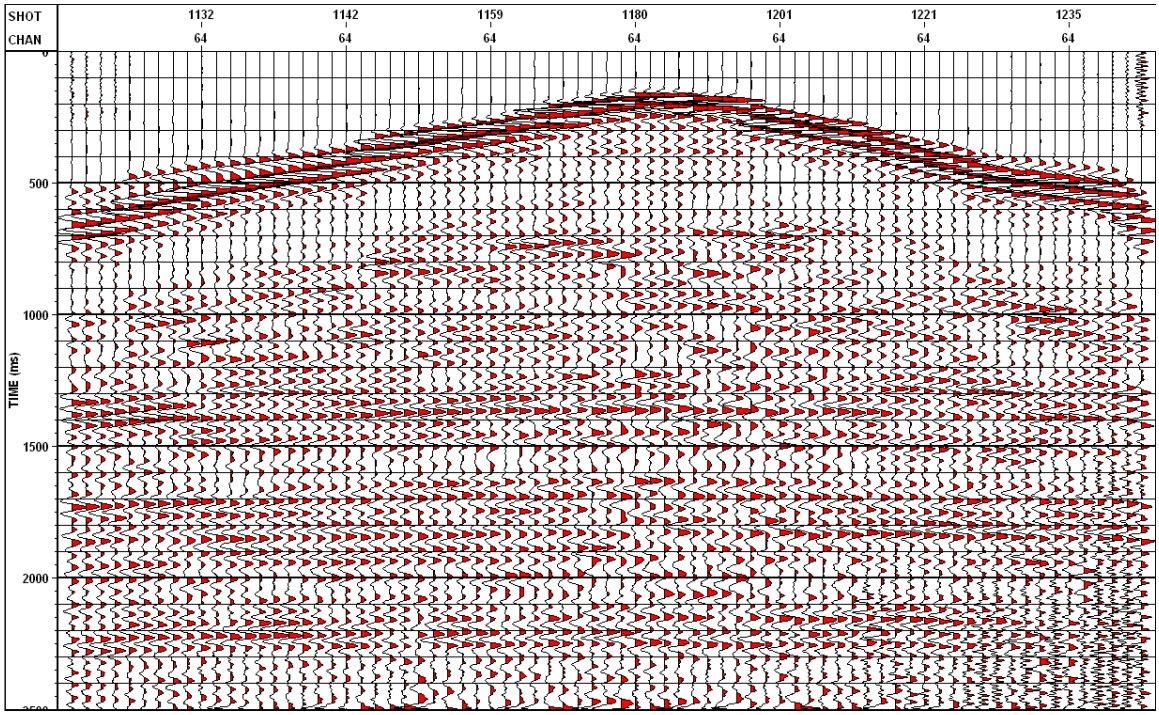

FIG. 19. Station 5183: IO-Spike vertical component, filtered 10-15-60-80 Hz with 500 ms window AGC applied for display.

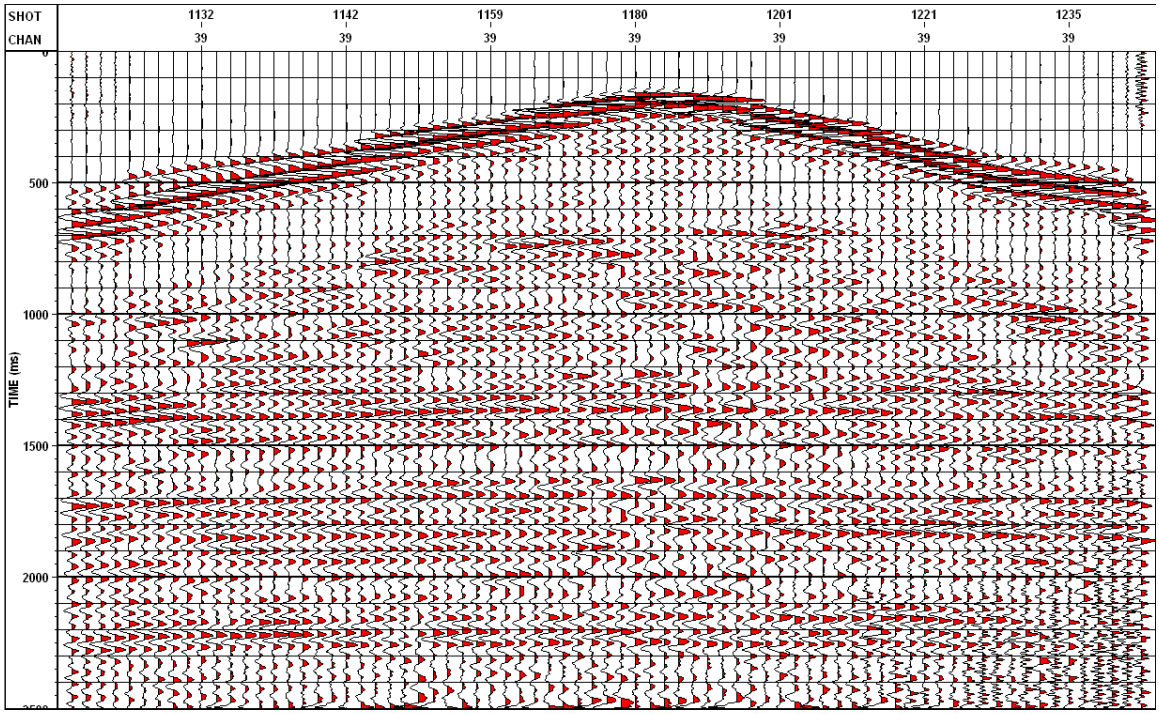

FIG. 20. Station 5183: GS-3C vertical component, filtered 10-15-60-80 Hz with 500 ms window AGC applied for display.

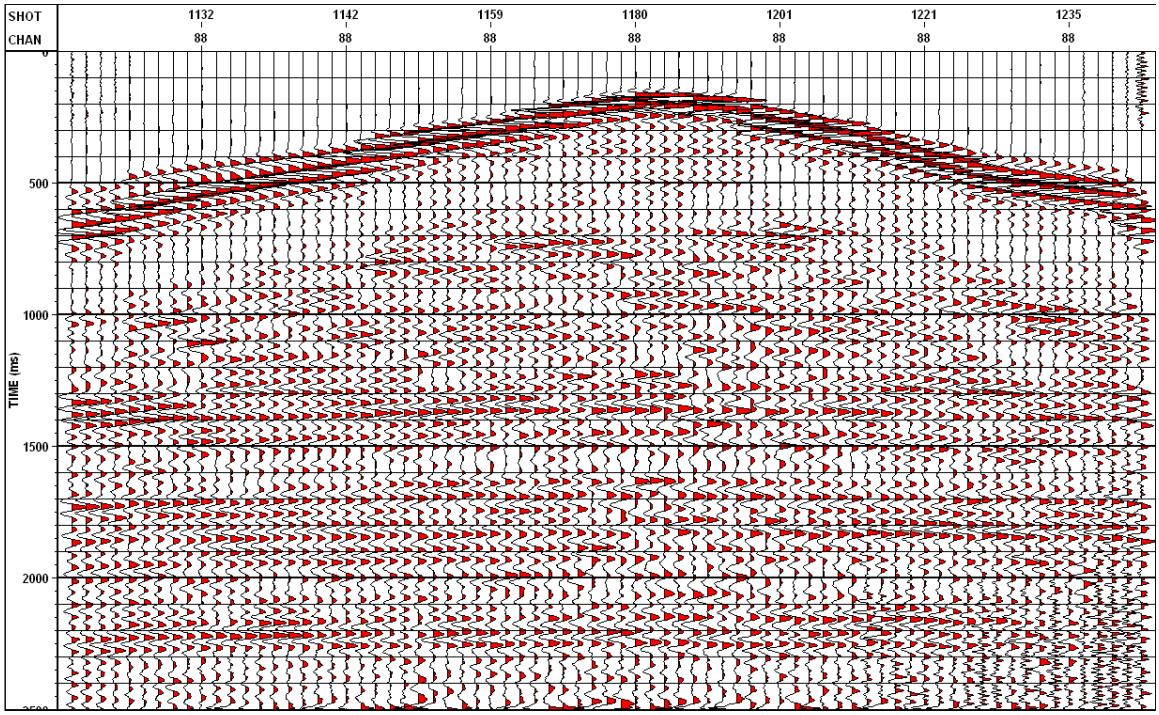

FIG. 21. Station 5183: OG-Nail vertical component, filtered 10-15-60-80 Hz with 500 ms window AGC applied for display.

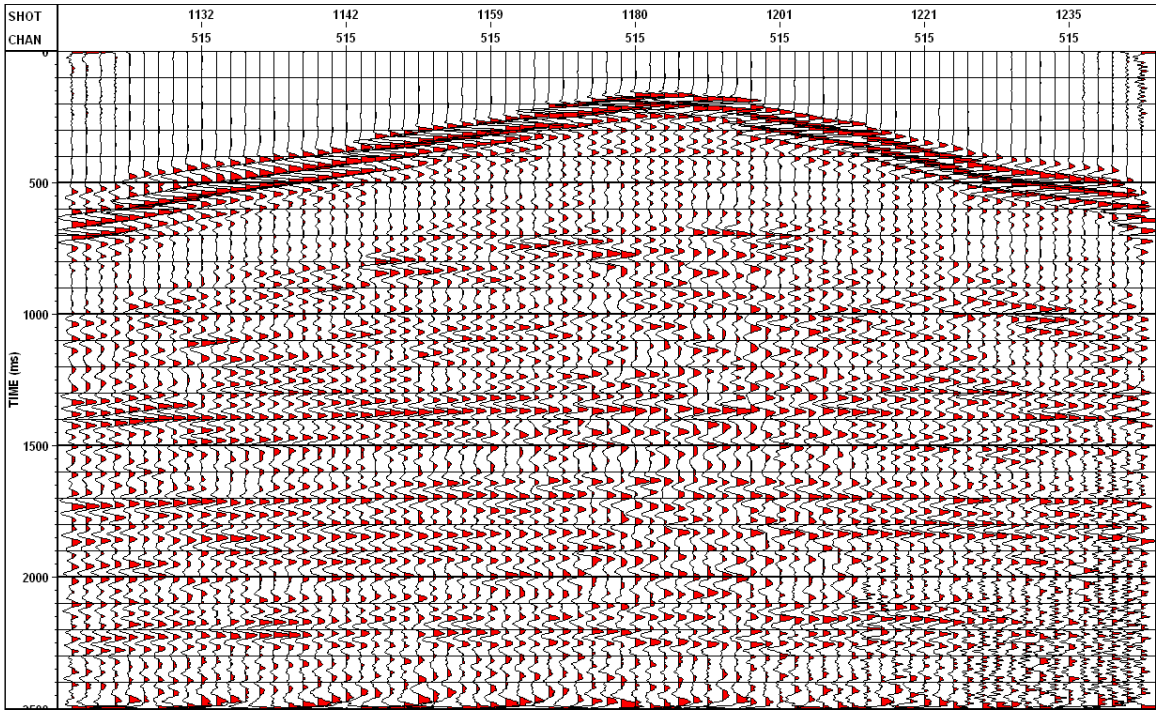

FIG. 22. Station 5183: Sercel-DSU3 vertical component, integrated, 90^{o} phase-shift applied, filtered 10-15-60-80 Hz with 500 ms window AGC applied for display.

Figure 23 shows a side-by-side view of part of the Sercel-DSU3 data after integration and a 90^o phase rotation and the equivalent part of the IO-Spike common receiver gather after a bandpass filter of 10-15-60-80 Hz has been applied. The first break and reflection data are extremely similar

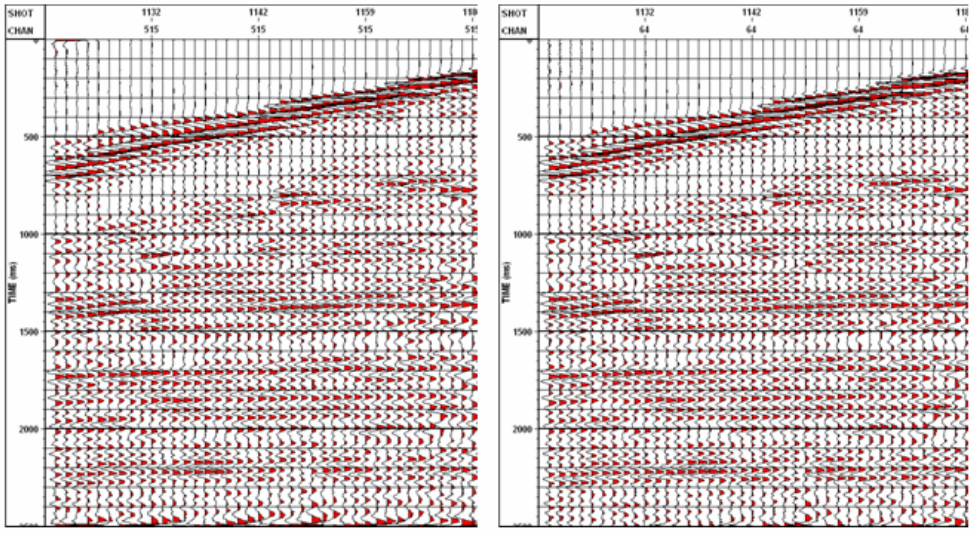

FIG. 23. DSU3 vertical-component gather after integration and 90^o phase shift (left) compared to equivalent traces from the IO-Spike gather (right). A bandpass filter of 10-15-60-80 Hz has been applied as well as AGC scaling with a 500 ms window for display.

Quantitative analysis

More quantitative comparisons between the datasets were also undertaken by examining amplitude spectra from all traces in the receiver gathers. Figure 24a shows amplitude spectra for raw data from all devices and shows approximately 10dB difference between the velocity and accelerometer data above 50 Hz, as expected. The deviation in the curves approaching Nyquist (250 Hz) is the response to the anti-alias filter in the Sercel-DSU3 instruments which were sampled at 2 ms (the coil geophones were all recorded at 1 ms and later resampled to 2 ms for analysis). Figure 24b shows amplitude spectra for the same datasets except after integration and application of a low-cut filter of 3 Hz to the Sercel-DSU data. The spectra are very similar above approximately 10 Hz, and Sercel-DSU shows higher amplitudes than the coil geophones below 10 Hz, as expected from the instrument response. Very similar results were obtained for data recorded at station 5184.

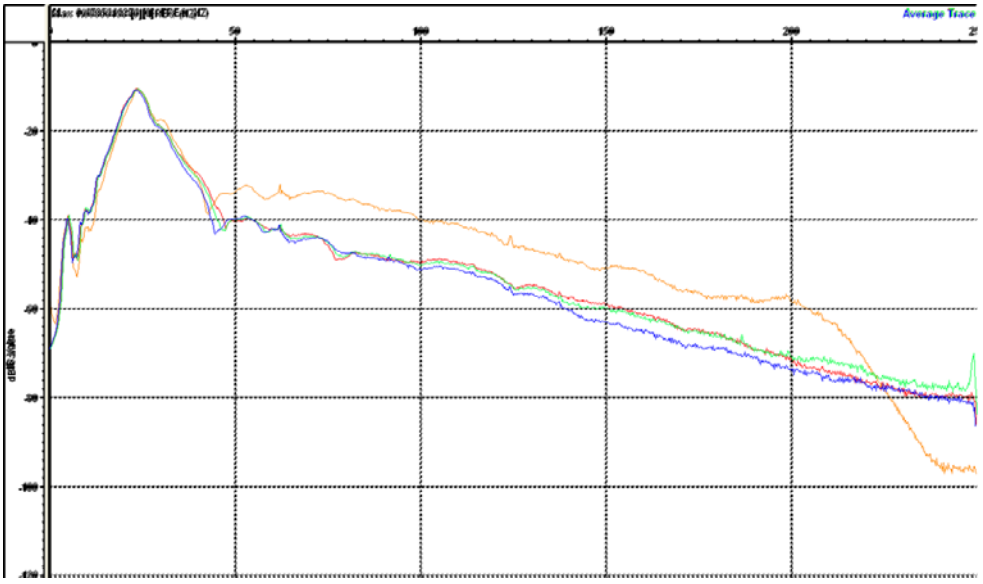

(a)

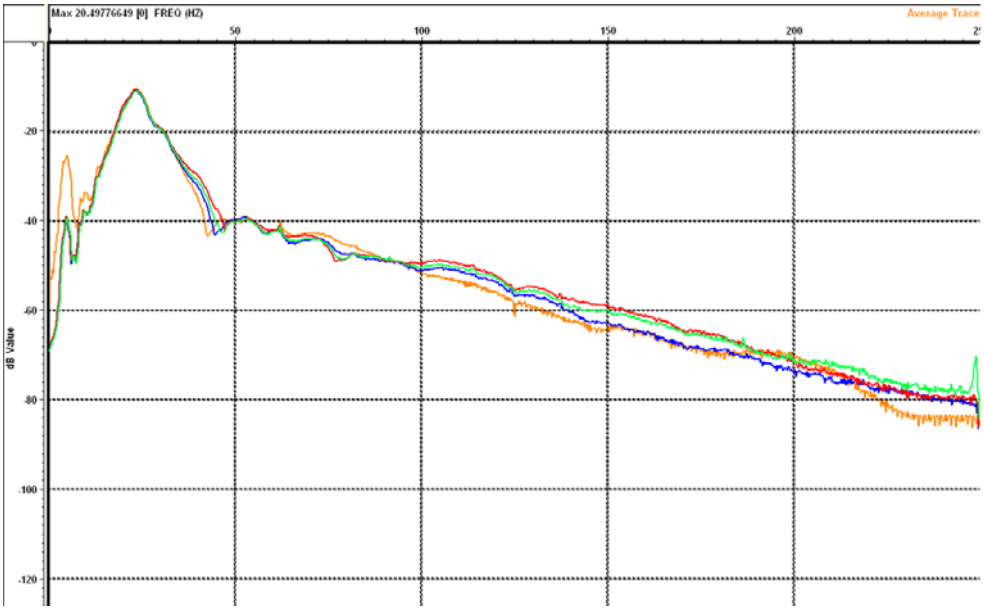

(b)

FIG. 24: Amplitude spectra for all devices at receiver station 5183. OG-Nail (red); IO-Spike (blue); GS-3C (green); Sercel-DSU3 (orange). (a) raw data. (b) after Sercel DSU data has been integrated and low cut filter of 3Hz applied.

Data displayed in Figures 19-22 were compared through a cross-correlation technique that applied a small shift to traces in order to find the maximum cross-correlation. For raw data, the cross-correlation was dominated by first break energy. After considerable experimentation, the most meaningful comparison were found by cross-correlating all traces of each gather after integrating the DSU3 data, applying a phase rotation of 90^{o}, then filtering all records with a bandpass filter of 10-15-60-80 Hz and applying AGC scaling with 500 ms window (Figure 25). The cross-correlation values lie mostly

between 0.9 and 1.0 with the overall greatest similarity between the various coil geophones, as expected. The correlation values between the Sercel-DSU3 data and the coil geophone data are only slightly smaller and are attributable to uncorrected phase characteristics of the geophone data.

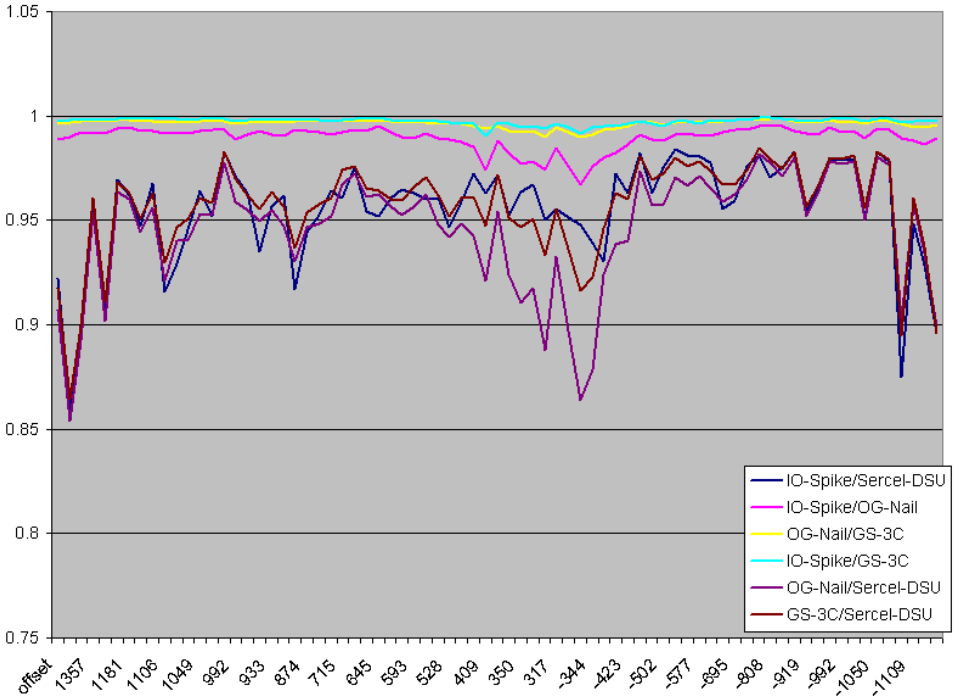

FIG. 25. Cross-correlation of records after Sercel-DSU3 data were integrated, phase rotated 90 degrees, then all records filtered 10-15-60-80 Hz and AGC applied (500msec).

Radial Component Data

As discussed previously, data from the recorded horizontal components were rotated into radial and transverse components, based on the known shot and receiver coordinates. Only a summary of the radial component data analysis is provided here. Figures 26 through 29 show the radial component data for the IO-Spike, GS-3C, OG-Nail and Sercel-DSU3 respectively, with the Sercel data having been integrated and phase-rotated to provide the best visual comparison. These displays have also been filtered with a bandpass of 10-15-60-80 Hz and have had AGC scaling with a 500 ms window applied for display purposes. The results indicate that the radial component data recorded by the all devices is very similar within the reflection frequency bandwidth. A high-amplitude converted-wave event is visible on all of the records with at about 700 ms. This event is from the Ardley coals that are at a depth of about 450 m at the site. It is noteworthy that during the rotation analysis it was found that the H1 and H2 components of the OG-Nail geophone had opposite polarity to the other two coil geophones, according to the arrow directions stamped on the top of the cases.

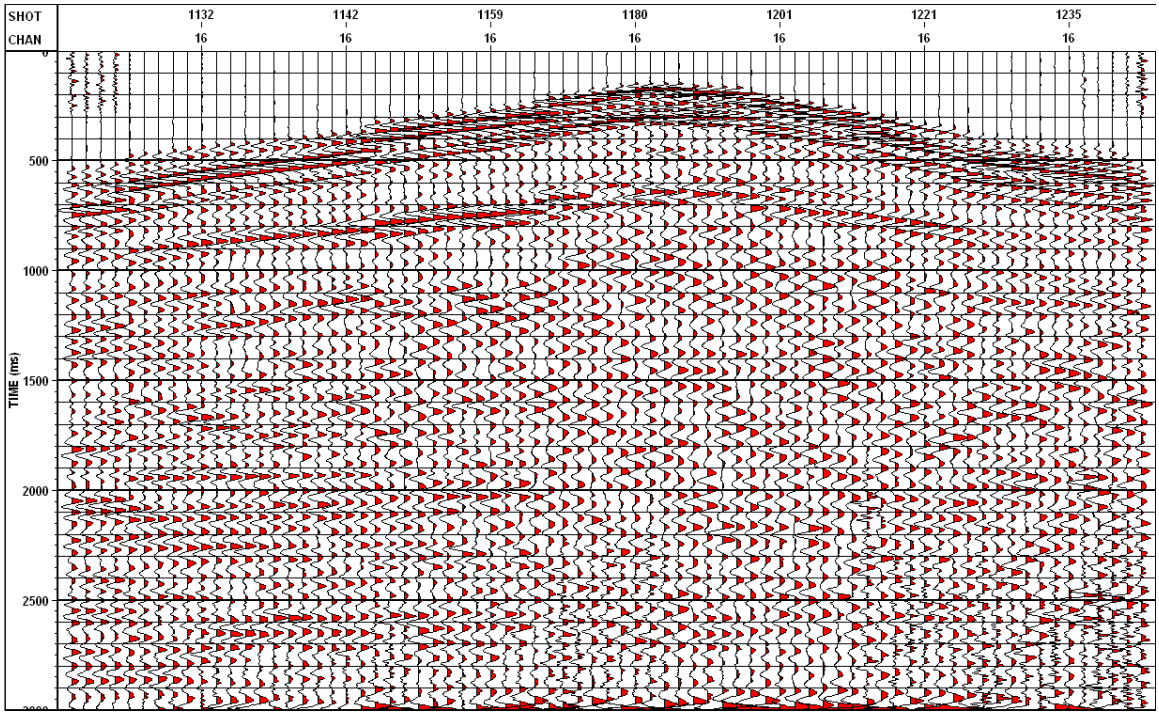

FIG. 26. Station 5183: IO-spike radial component, filtered 10-15-60-80 Hz with 500 ms window AGC applied for display.

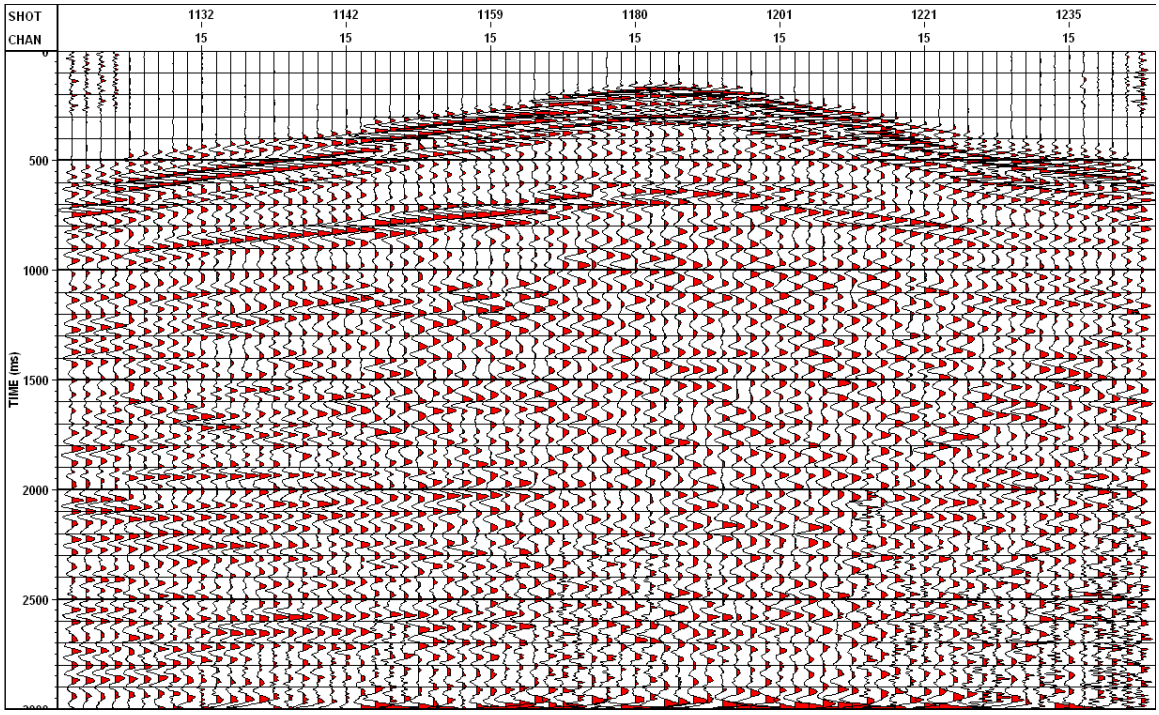

FIG. 27. Station 5183: GS-3C radial component, filtered 10-15-60-80 Hz with 500 ms window AGC applied for display.

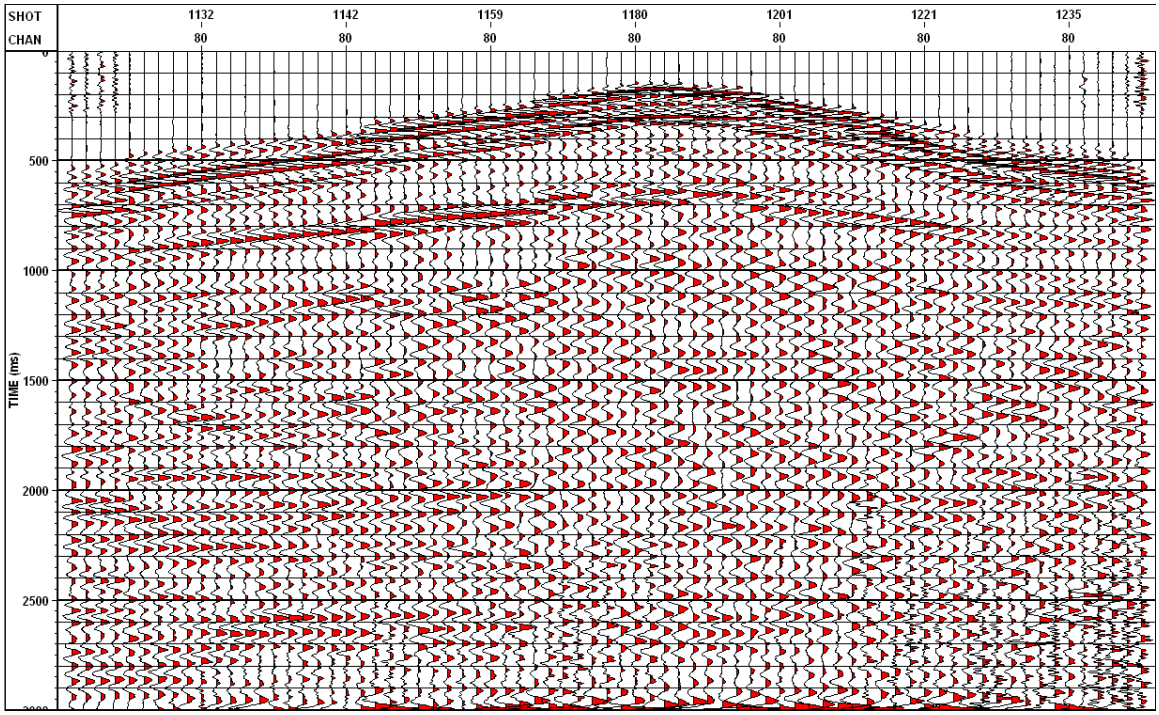

FIG. 28. Station 5183: OG-Nail radial component, filtered 10-15-60-80 Hz with 500 ms window AGC applied for display.

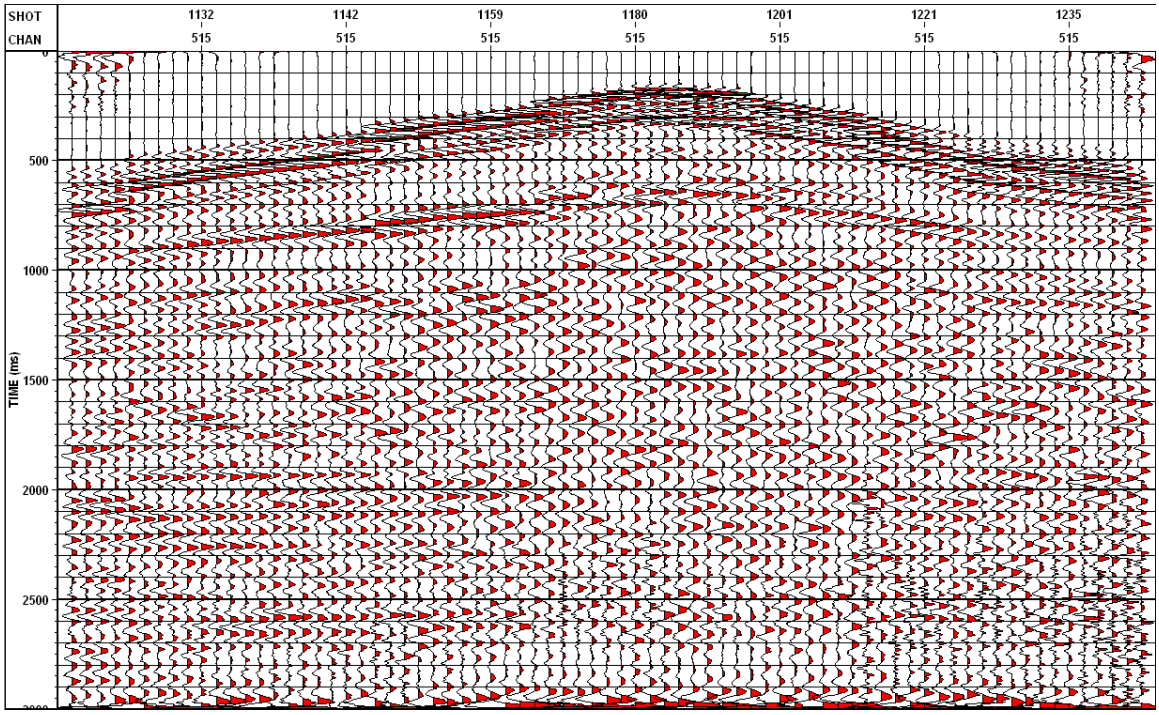

FIG. 29. Station 5183: Sercel-DSU3 radial component, integrated, 90^{o} phase-shift applied, filtered 10-15-60-80 Hz with 500 ms window AGC applied for display.

Figure 30 shows a side-by-side view of part of the Sercel-DSU3 radial-component data after integration and a 90^o phase rotation, and the equivalent part of the IO-Spike radial-component common receiver gather after a bandpass filter of 10-15-60-80 Hz has been applied. As for the vertical-component data, these records are also very similar

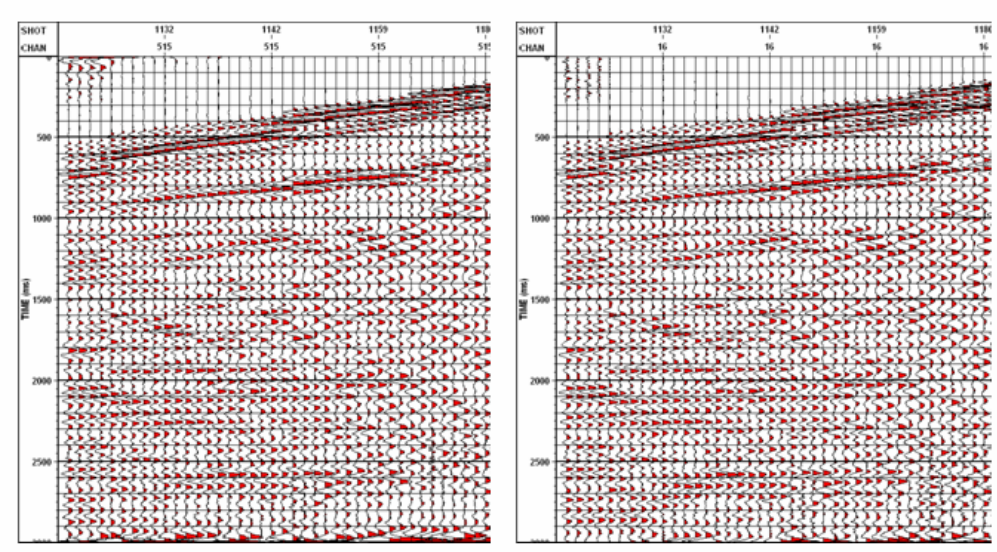

FIG. 30. DSU3 radial-component gather after integration and 90^o phase shift (left) compared to equivalent traces from the IO-Spike gather (right). A bandpass filter of 10-15-60-80 Hz has been applied as well as AGC scaling with a 500 ms window for display.

DISCUSSION AND CONCLUSIONS

This report has focussed on receiver gathers recorded at one receiver station. Our preliminary analysis shows similar results at all 8 receiver stations except that the overall data quality was found to vary between receiver stations. This variation is currently being investigated. In addition, the data will be processed to yield short receiver stacked sections, and the horizontal component data will be investigated for shear-wave splitting.

General conclusions from this study are:

- Vertical and radial components of common receiver gathers from all devices tested are virtually identical, regardless of the case shape and method of planting (e.g. spike vs augered hole). Data quality from all devices is high.

- The expected 90 degree phase difference between velocity and accelerometer data may not be discernable on raw data if the comparison is clouded by having different anti-alias filter types in the recording instruments. Also, the effect may also be due to uncorrected phase distortions in the geophone data across the signal bandwidth of the data recorded.

- The 90 degree phase difference and the "whiter" amplitude spectrum of the accelerometer data are handled by deconvolution. This is because a derivative is a minimum phase operator.

ACKNOWLEDGEMENTS

The Penn West CO_2 monitoring project is funded through the Alberta Energy Research Insitute (AERI), Western Economic Diversification (WED), Natural Resources Canada (NRCan), grants from the Natural Sciences and Engineering Research Council of Canada (NSERC) and support from the Consortium for Research in Elastic Wave Exploration Seismology (CREWES) at the University of Calgary, and Penn West Petroleum. The geophone data were collected using a seismic recording system owned by the University of Calgary with funding provided by the Government of Alberta and Nexen Inc. We also thank Fuju Chen, Yinbin Liu and Yongwang Ma for assisting with the field experiment.

We thank CREWES sponsors for supporting this research and GEDCO for providing access and support for VISTA which was used for processing and displaying the data presented in this report.

REFERENCES

Calvert, A. S., J. M. Novak, J. Maher, D. N. Burch, D. Bird, and R. Larson, 2005, A tale of two surveys: experiences processing two similar but different land 3D-3C MEMS surveys: 75th Annual International Meeting, SEG, Expanded Abstracts , 975-978.

Chen. F. and Lawton D., 2005, Interpretation of baseline surface seismic data at the Violet Grove CO_2 injection site, Alberta, CREWES Research Report, **17**.

Coueslan, M., Lawton D., and Jones, M., 2005, Baseline VSP processing for the Violet Grove CO_2 Injection Site, CREWES Research Report, **17**.

Coueslan, M., Lawton D., and Jones, M., 2006, The Penn West CO2 Injection Project: time-lapse monitoring with walkaway VSPs, CREWES Research Report, **18** (this volume).

Gibson, J., and R. Burnett, 2005a, Another Look at MEMS Sensors and Dynamic Range: Recorder, **30** , no.2, 44-47.

Gibson, J., R. Burnett, S. Ronen, and H. Watt, 2005b, MEMS sensors: Some issues for consideration: The Leading Edge, **24** , no.8, 786-790.

Hons, Michael S. and Stewart, Robert R., 2006, Transfer functions of geophones and accelerometers and their effects on frequency content and wavelets, CREWES Research Report, **18** (this volume).

Mougenot, D., and N. Thorburn, 2004, MEMS-based 3D accelerometers for land seismic acquisition: Is it time?: The Leading Edge, **23** , no.3, 246-250.

Ronen, S., L. Comeaux, M. Cartwright, J. B. Gibson, R. Burnett, J. Roy, and H. J. Watt, 2005a, Comparison between geophones and two MEMS types and repeatability of land data: 75th Annual International Meeting, SEG, Expanded Abstracts , 908-911.

Ronen, S., J. Gibson, R. Burnett, J. Roy, B. Montgomery, R. Kendall, L. Comeux, and H. Watt, 2005b, Comparison of Multi-Component Data from Different MEMS Sensors: 67th Meeting, EAGE, Expanded Abstracts , B021.

Tessman, J., B. Reichert, J. Marsh, J. Gannon, and H. Goldberg, 2001, MEMS for geophysicists: 71st Annual International Meeting, SEG, Expanded Abstracts , 21-24.